Hindawi
Advances in Civil Engineering
Volume 2021, Article ID 4813415, 13 pages
https://doi.org/10.1155/2021/4813415

Research Article

Application of Ground Penetrating Radar in Detecting Deeply Embedded Reinforcing Bars in Pile Foundation

Daochuan Zhou[1] **and Haitang Zhu**[2]

[1]*Department of Civil Engineering and Architecture, Jiangsu University of Science and Technology, Zhenjiang, China*
[2]*College of Civil Engineering, Henan University of Engineering, Zhengzhou, China*

Correspondence should be addressed to Daochuan Zhou; dczhou@just.edu.cn

Received 16 October 2019; Revised 22 January 2021; Accepted 8 April 2021; Published 19 April 2021

Academic Editor: Meng Gao

Ground penetrating radar (GPR) has been widely used for nondestructive testings in civil engineering. However, the GPR has not been adequately applied in detecting deeply embedded reinforcing bars, which is usually difficult to be revealed in radar image due to the wave interference and attenuation in large depth penetration. This study presents a new approach for the GPR detection of deeply embedded reinforcing bars in the reinforced concrete pile foundation. The aim of the GPR survey is to determine the existence and the depth of internal reinforcing bars in the pile foundation for solving engineering dispute. Low centre frequency antenna was used in GPR field testing to obtain the reflected raw data. Optimized procedures of digital filtering techniques were applied to process the GPR raw data. The deeply embedded reinforcing bars are revealed in the radar image after the field testing and postprocessing procedures. The depth of the reinforcing bars was estimated based on the hyperbola match method. The GPR test results were validated by the excavation of the pile foundation. The low centre frequency antenna has been found to be essential to obtain the reflected wave signals of deeply embedded reinforcing bars. The optimized processing procedures is useful to identify and display the reinforcing bars in radar image. The combination of low centre frequency antenna and the post-processing procedures make the detection of deeply embedded reinforcing bars feasible. The proposed GPR testing method has been found to be effective to estimate the depth of deeply embedded reinforcing bars, which provides the key information for solving engineering dispute.

1. Introduction

Ground penetrating radar (GPR) is a high frequency electromagnetic wave technology, which was initially used in the geophysical engineering for shallow subsurface investigations. Two antennas are usually used to emit and receive electromagnetic wave signals. The electromagnetic wave signals are transmitted by the emitting antenna to propagate into the inspecting medium. Some of the emitted wave signals are scattered and reflected during the propagation in the inner space of the inspecting medium. Reflections of the wave signals often occur at the interfaces of two materials with different electromagnetic properties. The remaining wave signals continue to propagate towards the deeper space of the medium. The reflected wave signals are recorded and amplified by the receiving antenna. Different wave traces can be obtained with the information including two-way propagation time, wave frequencies, and amplitude characteristics. By processing and analysing the received wave signals, the buried objects in the inspecting medium can be revealed in the radar image. Hence, the information of the buried objects can be obtained in a nondestructive and noninvasive way.

As a popular nondestructive testing technology, the GPR has been widely used in civil engineering for inspecting and diagnosing concrete structures during the last three decades [1]. The GPR has been used to investigate the thickness of the bituminous pavement [2], bridge reinforcements and tunnel lining [3, 4], location of steel bars in reinforced concrete (RC) members [5–7], location of voids and cracks in concrete members and concrete foundation [8, 9], the thickness of concrete cover in reinforced concrete members [10], size

of reinforcing bars [11, 12], and corrosion of reinforcing bars [13, 14]. The GPR applications in concrete structures have been reviewed by Wallace [1] and Bungey [15].

The GPR detection of reinforcing bars focused on the shallow embedded reinforcing bars, which were located near the surface of concrete members, usually not exceeding 0.3 m. However, reinforcing bars are buried in deep position in some circumstances. The GPR has not been reported to detect the deeply embedded reinforcing bars. Some difficulties may arise in this case. The wave signals can be partially reflected due to the objects above the reinforcing bar. The reflection of the above objects minimizes some of the radar waves propagating into the deeper space of the inspecting medium. Also, the reflected wave signals of the reinforcing bars are weakened due to the loss and attenuation in the process of large depth penetration. The unfavorable condition can mask the GPR detection results of the deeply embedded reinforcing bars and make the interpretation of the results significantly difficult. Due to these difficulties, the GPR has not been adequately used to detect deeply embedded reinforcing bars in RC structures.

This study presents a new approach of the GPR to detect the deeply embedded reinforcing bars in a RC pile foundation. The new approach involves GPR field testing, processing of GPR raw data, and validation of the GPR detection results. The study shows that the new approach is effective in detection of the deeply embedded reinforcing bars.

2. The GPR Testing of RC Pile Foundation

Large diameter pile foundations are one of the most important underground structures that are widely used in high-rise buildings. The GPR has been used to determine the length of pile [16], the buried footings, as well as concrete foundation elements [17] and the inclination of pile foundation [18]. However, the GPR application of detecting the reinforcing bars in the pile foundation has been limited. The examination of internal reinforcing bars in the pile foundation is necessary after construction, which has traditionally been carried out by drilling and excavating as intrusive investigations with the limitation of considerably expensive and time-consuming. It also causes some degree of damages to the structure. Moreover, only discrete data can be obtained by the intrusive investigation. In order to avoid the damage to the structure and obtain continuous inspection results, the proper use of the GPR is essential. The use of the GPR could minimize the cost for repair, inspection, and maintenance of the structure.

The reinforcing bars should be exposed on the surface of the pile foundation after construction, as shown in Figure 1(a), showing the detailed information of reinforcements for postconstruction inspection. However, in some cases, the protruding reinforcing bars could be different from the original design requirement, or some of reinforcing bars could be even missing due to the poor management of construction. Figure 1(a) shows the normal pile foundation after construction, where the reinforcing bars can be seen on the surface of the pile foundation for postconstruction inspection. In contrast, Figure 1(b) shows a problematic pile foundation, where reinforcing bars are missing on the surface of the pile foundation. The problematic pile foundation needs to be investigated to confirm the existence of the internal reinforcing bars. The information of the internal reinforcing bars is very important for solving the engineering dispute between the construction unit and the supervision unit. The dispute between the two units focuses on whether the reinforcing bars are used or not in the construction process. The GPR testing could provide the information of the internal reinforcing bars for solving the engineering dispute and help to make decision of further treatment of the problematic pile foundation.

In this study, a new approach of the GPR detection of deeply embedded reinforcing bars in the pile foundation is presented. The approach involves the GPR field testing, postprocessing procedures, and validation of the GPR testing results. The GPR field testing of the RC pile foundation was performed by using low centre frequency antenna. The GPR raw data were obtained, which is processed by using the optimized procedures of digital filtering techniques. A nonintrusive hyperbola match method was used for the estimation of the wave velocity in the pile foundation. The time-depth conversion of GPR image was performed based on the estimated wave velocity. The estimated depth of the reinforcing bars is validated by excavating the pile foundation. It has been demonstrated that the new approach of GPR testing is effective in the detection of the deeply embedded reinforcing bars. The validated information of the deeply embedded reinforcing bars is used for solving the engineering dispute by demolishing the pile foundation partly and recasting.

3. Theory and Methods

3.1. GPR Theory for Evaluation of RC Structure. The purpose of GPR detecting of RC structure is to obtain the information of internal reinforcing bars and concrete materials. The information of internal reinforcing bars includes the position, the cover length, and the size of bars. The cover length of the reinforcing bars is equal to the depth of the embedded bars in concrete materials. The depth estimation of reinforcing bars is influenced by the wave propagation velocity in the inspecting concrete medium. The velocity of electromagnetic waves in the solid medium can be expressed as

$$v = \frac{c}{\sqrt{\varepsilon_r \mu_r \left(1 + \sqrt{1 + \eta^2}/2\right)}}, \quad (1)$$

where v is the wave velocity in the inspecting medium, c is the constant value of wave velocity in the vacuum ($c \approx 30$ cm/ns), and η is the loss factor. Concrete is considered as a low loss and a nonmagnetic material. The relative magnetic permeability (μ_r) of concrete is 1. For low loss materials, the loss factor, η, is equal to 0. Substituting the two parameters ($\mu_r = 1$, $\eta = 0$) into equation (1), the wave velocity in concrete material can be simplified as

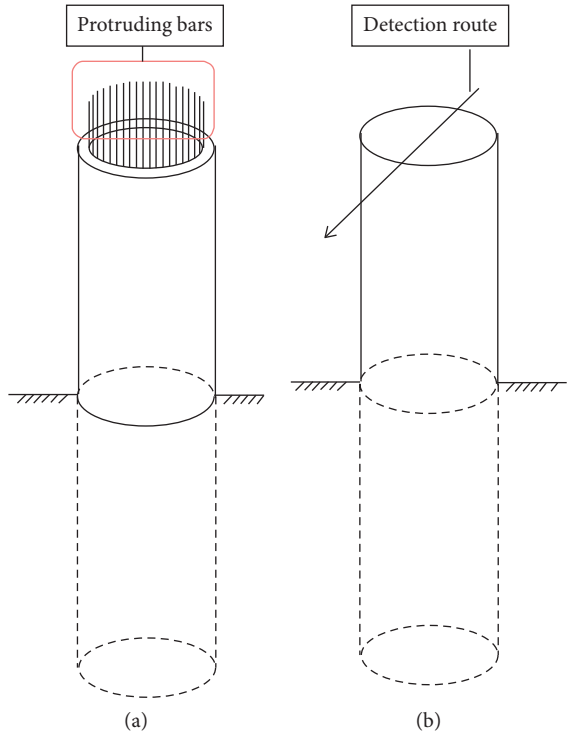

Figure 1: Pile foundation after construction. (a) Normal case with protruding bars and (b) the test pile foundation.

$$v = \frac{c}{\sqrt{\varepsilon_r}}, \tag{2}$$

where v is the wave velocity in concrete medium. From equation (2), the wave velocity in concrete material depends on the relative dielectric permittivity (ε_r) of the concrete material. The wave velocity is inversely proportional to the square root of the relative dielectric permittivity and decreases with the increase in the relative dielectric permittivity. Table 1 provides the electromagnetic parameters of construction materials. The relative dielectric permittivity is 1 for air and 81 for fresh water. The relative dielectric permittivity of concrete materials typically lies between 4 and 20, depending on the moisture content, ambient temperature, and the wave frequency. The wave velocity in the concrete medium lies between 6.7 cm/ns and 15 cm/ns. The concrete with higher moisture content possesses lower wave velocity.

The energy of the electromagnetic wave is reduced during the penetration because of the wave attenuation. The attenuation influences the penetration depth. The wave attenuation is influenced by the effective electrical conductivity, dielectric permittivity, and wave frequency. The attenuation increases with the increase of the wave frequency, moisture content, and dissolved salts. The attenuation is proportional to the electrical conductivity. High attenuation occurs in the medium with high electrical conductivity, such as steel and other metals. The larger depth penetration is only possible in the condition of lower wave frequency.

The GPR has a broad range of frequency components typically in the range of 10–5000 MHz. The GPR wave with different centre frequencies provides different capabilities of penetration depth and scale. The penetration depth of the GPR is influenced by the centre frequency of the wave signals, electrical conductivity of the medium, and the wave attenuation. In low loss materials, the detectable depth increases as the wave frequency decreases, while high centre frequency radar waves yield a reduced penetration depth. Electromagnetic waves in low centre frequency enable detecting underground foundations in a large depth.

The vertical resolution of the GPR depends on the wavelength (λ) of the electromagnetic waves, as expressed in the following equation.

$$\lambda = \frac{v}{f}, \tag{3}$$

where v is the wave velocity in the inspecting medium, and f is the centre frequency of electromagnetic waves. For a given centre frequency, the detectable distance between two reflectors must be greater than half of the wavelength. The vertical resolution increases as the centre frequency of radar waves increases.

The horizontal resolution depends on the antenna radiation pattern, centre frequency of radar waves, depth of the embedded target, and electromagnetic parameters (e.g., the number of scans per second). The horizontal resolution can be determined as

$$d_h = \sqrt{\lambda d_t}, \tag{4}$$

Table 1: Electromagnetic parameters of construction materials [11].

Material	Relative dielectric permittivity, ε_r	Wave velocity, v (cm/ns)	Relative conductibility, μ_r (S/m)
Air	1	30	10^{-10}
Freshwater	81	3.3	$10^{-4} \sim 3 \times 10^{-2}$
Dry sand	3–6	12.2–17.3	$10^{-7} \sim 10^{-3}$
Cement	5	13.4	
Gravel	6	12.2	
Concrete	4–20	6.7–15	
Plastic (PVC)	3.3	16.5	1.34
Iron	300	0	$10^{7} \sim 10^{10}$

where d_h is the detectable horizontal distance, and d_t is the actual depth of the embedded target in the concrete medium.

3.2. The Formation of Hyperbolic Signature in Radar Image. The two-dimensional reflected radar images are used in analysis for evaluation of RC structure after GPR field testing. In the two-dimensional GPR scan (Figure 2), electromagnetic waves propagate into the concrete host medium in an elliptical cone with the apex of the cone at the centre of the emitting antenna. This elliptical cone is usually elongated parallel to the direction of the GPR scan along the concrete surface. As shown in Figure 2, the energy radius of GPR waves changes in different depths of the concrete medium. The elliptical cone of the GPR detection indicates that all objects inside the elliptical cone can be detected by recording the reflected wave signals. However, when the embedded object is outside of the elliptical cone, no reflected signals of the object can be recorded. When the two-dimensional GPR scan is performed, the antenna moves along the scan direction, which is orthogonal to the axis of the reinforcing bar. Continuous GPR data are obtained, consisting of wave traces in different amplitudes. Each of these traces contains a series of waves that vary in amplitude. The magnitude of the amplitude depends on the amount and intensity of wave signals that are reflected at the interfaces of the concrete host medium and the embedded objects.

Equation (5) estimates the energy radius in different depths of the host medium [12], which is based on the relative dielectric permittivity (ε_r), wavelength (λ), and vertical distance (H) from the concrete surface to the given depth.

$$\frac{E}{2} = \frac{\lambda}{4} + \frac{H}{\sqrt{\varepsilon_r + 1}}, \tag{5}$$

where E is the energy footprint, which is the size of the diameter of the energy area at the given depth, and $E/2$ is the energy radius.

The reinforcing bar is a cylindrical object buried in the concrete members. When electromagnetic waves in the edge of the elliptical cone propagate into the interface of the concrete and the reinforcing bar, the reflected wave signals of the reinforcing bar are recorded as from beneath the antenna. The radar antenna always operates in conical beams. The reflected wave signals can be recorded, even though the antenna is not directly over the reinforcing bar. Detected from a number of different angles, the reinforcing bar is always recorded as if it were directly underneath the location of each trace. The presence of the reinforcing bar is revealed in radar image as the wave reflection with different amplitudes in different traces. The different traces of the received wave signals provide the characteristic hyperbolic signature in radar image, which is considered as the evidence of the existence of the internal reinforcing bar in the concrete host medium, as shown in Figure 3(c). The radar image of GPR two-dimensional scan with different traces is shown in Figure 3(b), which is created by the reflection of wave signals that occurs on the boundary of the cylindrical object with changing distance between the antenna and the object.

3.3. Mathematical Model of the Hyperbolic Signature. In the two-dimensional GPR scan, the antenna keeps moving straight in one-direction at the surface of the host medium. The distance between the antenna and the embedded reinforcing bar is changing as the antenna moves. The location of the antenna is described by two parameters: x_i and z_i. The x_i is the antenna position on the surface of the concrete medium, and z_i is the distance from the antenna position x_i to the boundary of the reinforcing bar, as shown in Figure 3(a). For the simplicity in the calculation and to reduce the complexity of the inversion problem of the wave velocity, the reinforcing bar is simplified as a point reflector. The radius of the reinforcing bar is omitted in the mathematical model of the hyperbolic signature. Also, the distance between the emitting antenna and receiving antenna is neglected. Based on these assumptions, the geometrical relationship can be written as

$$z_i^2 = z_0^2 + (x_i - x_0)^2, \tag{6}$$

where z_0 is the distance from the antenna horizontal location x_0 to the boundary of reinforcing bar. The x_0 is the horizontal position above the reinforcing bar. The distance z_0 represents the depth of the reinforcing bar which is equal to the thickness of the concrete cover. The distances z_i and z_0 can be calculated by the product of the wave velocity and half of the two-way propagation time, as in the following equation.

$$\begin{cases} z_i = v\dfrac{t_i}{2} \\ \\ z_0 = v\dfrac{t_0}{2} \end{cases}, \tag{7}$$

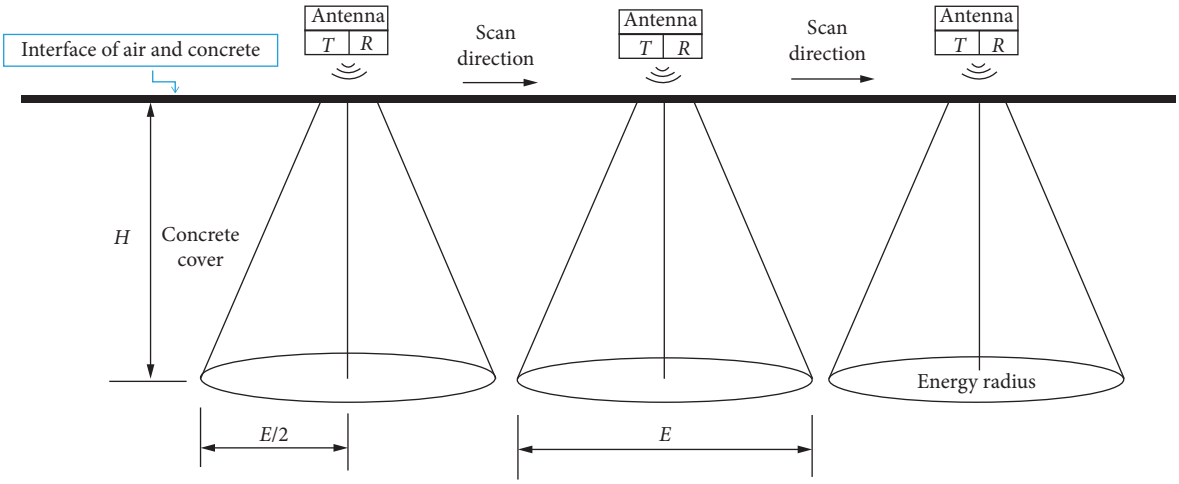

FIGURE 2: The elliptical cone of GPR waves propagating into the inspecting medium. Note: T, transmitting antenna; R, receiving antenna; E, energy diameter; E/2, energy radius; H, thickness of concrete cover.

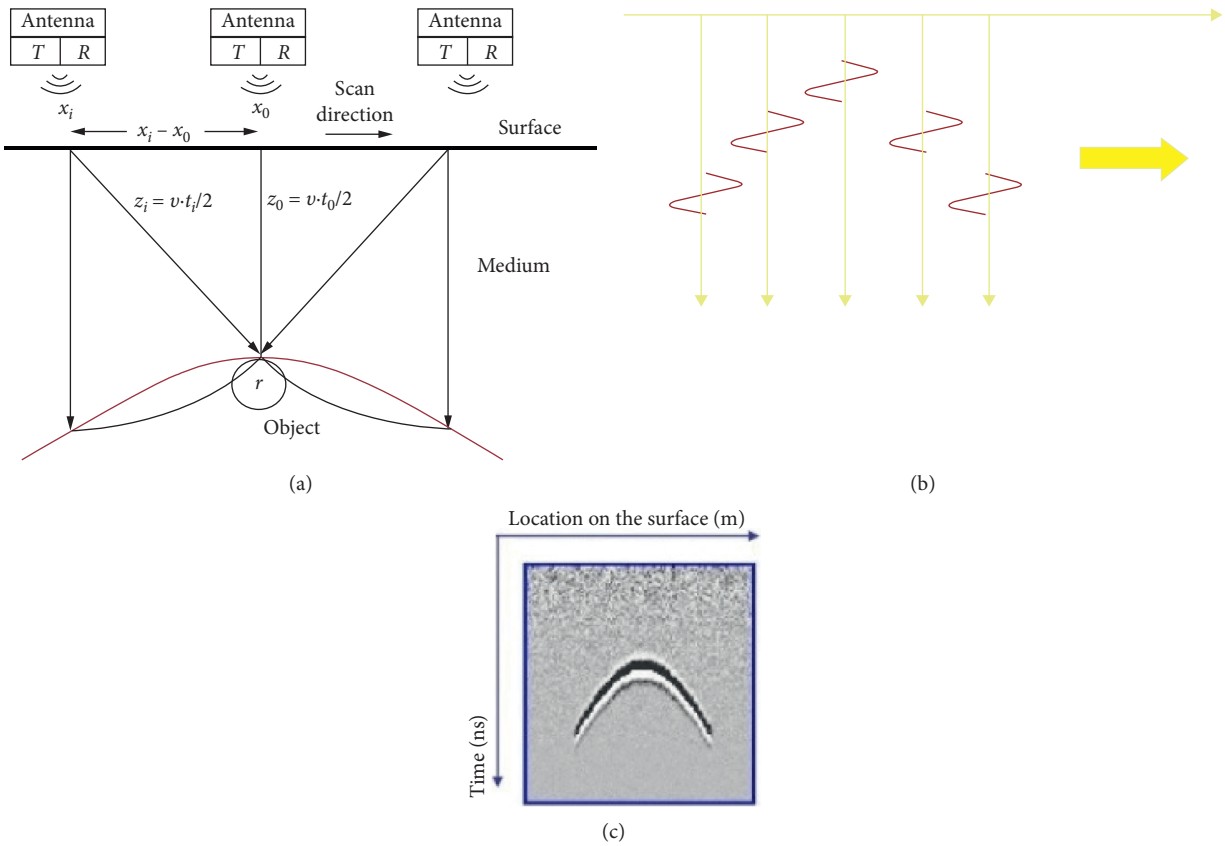

FIGURE 3: The formation of hyperbolic signature in the radar image. (a) Geometrical characteristics of a buried reinforcing bar in concrete, (b) radar wave traces, and (c) hyperbolic signature of the reinforcing bar.

where t_i is the two-way propagation time between the antenna location x_i to the boundary of the embedded reinforcing bar. The t_0 is the two-way propagation time between the antenna location x_0 to the surface of the embedded reinforcing bar. Substituting the distances z_i and z_0 into equation (6), the simplified hyperbolic equation can be written as

$$\left(\frac{t_i}{t_0}\right)^2 - \left(\frac{x_i - x_0}{vt_0/2}\right)^2 = 1. \quad (8)$$

The GPR evaluation of the pile foundation focuses on detection of the embedded reinforcing bar and estimating the depth of the reinforcing bar. The size of the reinforcing

bar is not in the target of the GPR field testing. Hence, the reinforcing bar is assumed to be a point reflector. The radius of the reinforcing bar is assumed to be zero. The hyperbolic model in equation (8) is based on the assumption of the point reflector. Additionally, the inspecting concrete medium is assumed to be a homogeneous material, and the wave velocity in the concrete medium is considered to be a constant. These assumptions provide convenience in the calculation process of the depth of the reinforcing bar. The process becomes much easier due to the simplification of zero radius reinforcing bar. The hyperbolic equation (8) can be written as a function of t_0, x_0, x_i, and v as

$$t_i = \sqrt{t_0^2 + \frac{4\left(x_i - x_0\right)^2}{v^2}}, \tag{9}$$

where (x_0, t_0) is the peak coordinate of the hyperbolic reflection, which can be extracted from the first positive peak amplitude of the hyperbolic signature in the radar image. The parameter t_i is the longitudinal coordinate corresponding to the horizontal coordinate x_i. The model of two-way propagation time in equation (9) is a standard equation of a hyperbola.

3.4. Estimation of the Depth of the Embedded Reinforcing Bar. The depth of the embedded reinforcing bar is related to the two-way propagation time t_0, as expressed in the following equation.

$$D = v\frac{t_0}{2}, \tag{10}$$

where D is the vertical depth from concrete surface to the boundary of the embedded reinforcing bar. The key point in the estimation is the determination of the wave velocity (v) in the concrete host medium. Based on the assumption that concrete is a homogeneous material, the wave velocity in the concrete medium is considered to be a constant. The hyperbola match method is used to determine the wave velocity. The problem of retrieving the wave velocity from the GPR raw data has a unique theoretical solution that can be obtained by data fitting of the hyperbolic curves, as in the following equation.

$$t = \sqrt{t_0^2 + \frac{4\left(x - x_0\right)^2}{v^2}}. \tag{11}$$

Equation (11) can be written as equation (12), as a function of four parameters:

$$t = t\left(x_0, t_0, v, x\right). \tag{12}$$

For determining the wave velocity, a set of data points (x_i, t_i) can be extracted from the hyperbolic signature by selecting only the first positive peak amplitude. The total number of points is n. The square of the absolute error related to the points (x_i, t_i) is given by

$$\eta_i^2 = \left(t - t_i\right)^2 = \left[t\left(x_0, t_0, v, x_i\right) - t_i\right]^2. \tag{13}$$

To determine the unknown wave velocity by the least mean square method, the fitness function is defined as

$$\sum_{i=1}^{n} \eta_i^2 = \sum_{i=1}^{n} \left[t\left(x_0, t_0, v, x_i\right) - t_i\right]^2. \tag{14}$$

By choosing continuous values of the relative dielectric permittivity in the range of concrete materials (Section 3.1), different wave velocities can be obtained from equation (2). As a result, hyperbolic curves corresponding to the wave velocities can be generated from equation (11). By minimizing the sum of square errors between the hyperbolic curves and the set of extracted points, the wave velocity in the concrete medium can be determined according to equation (14). As a result, the depth of the reinforcing bar can be estimated by the determined wave velocity and the two-way propagation time, as expressed in equation (10).

4. GPR Equipment and the Data Acquisition Process

4.1. GPR Equipment. The RIS K2 FastWave radar system manufactured by the IDS GeoRadar [19] was used to perform the two-dimensional GPR scan of the problematic pile foundation. Multichannel and multifrequency antennas are available in the RIS K2 FastWave radar system, which greatly improved the accuracy and the clarity of the mapping. The RIS K2 FastWave radar system is composed of digital antenna driver (DAD) control element, antennas, notebook computer, cables, battery, and software.

The RIS K2 FastWave radar involves the signal launching system, signal receiving system, signal conversion system, and signal postprocessing system, as shown in Figure 4. The signal launching and receiving systems are made up of antennas, the DAD control element, and data acquisition software, battery, and cables. The reflected electromagnetic wave signals are transformed into digital signals in the DAD control element and transmitted to the notebook computer through the intranet. The postprocessing of the digital signals is carried out using the processing software. Postprocessing procedures of the digital signals are described in Section 5.

The DAD control element is the core processing unit of the radar system. The DAD control element activates launching and recording radar wave signals and converts the recorded wave signals into digital signals. The processing software [20] is used to process the digital signals with the function of visualizing, filtering, and analysing. All elements are connected to the corresponding ports of the DAD control element through cables. The connection of the DAD control element is shown in Figure 5.

Antennas are named using the centre frequency of the emitting electromagnetic waves. Three different types of antennas are available for different depth penetration of the inspecting medium. In this study, the TR80 antenna was used with a lowest centre frequency of 80 MHz, which can detect 20–40 meters depth in rock material, as shown in Figure 6. The TR80 antenna enables the large depth

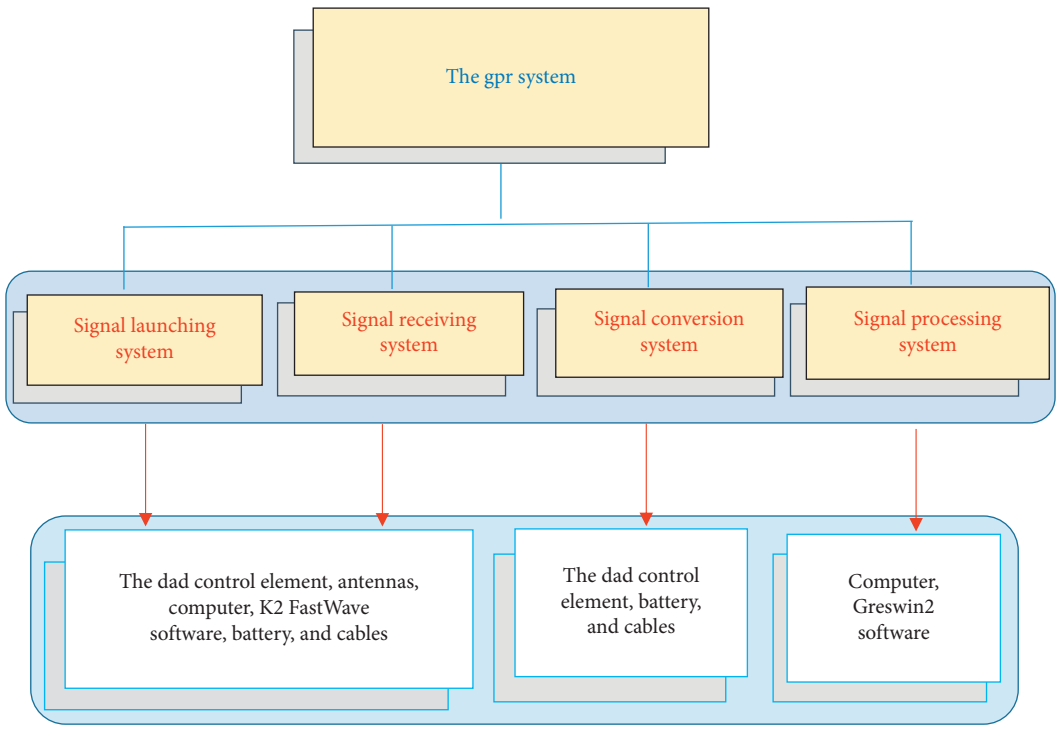

Figure 4: The GPR system.

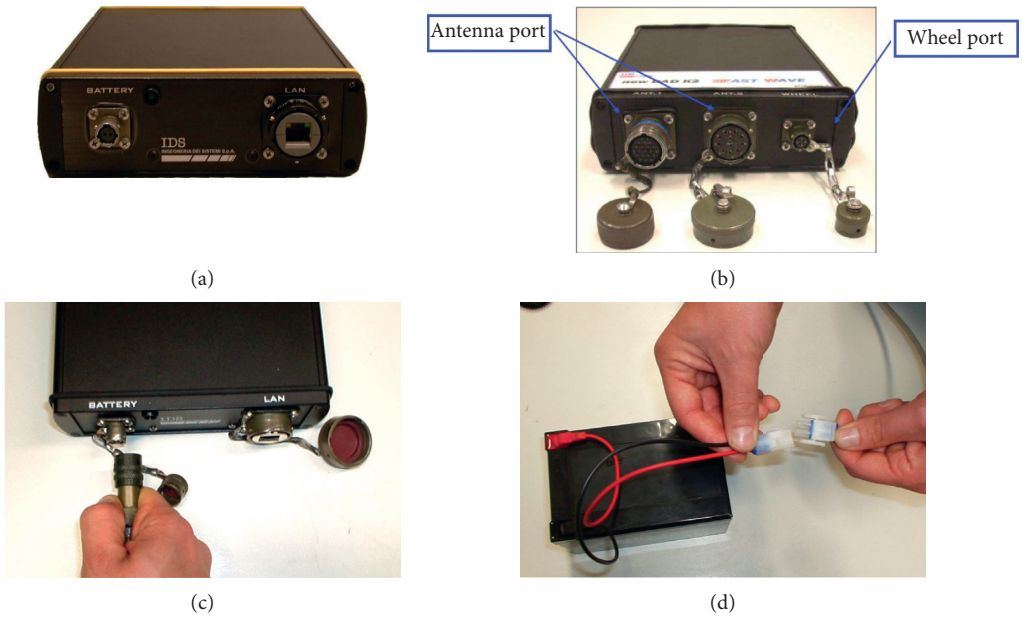

Figure 5: The DAD control element and connections. (a) Battery and LAN port on the one side of the DAD control element, (b) antenna port and wheel port on the other side of the DAD control element, (c) battery cable connected to the battery port, and (d) connection of the power energy of a sealed lead acid battery.

penetration in concrete material, which consist of two essential antennas for launching and recording wave signals during the GPR survey. In the GPR field testing of the pile foundation, the two antennas are placed close to each other, and the distance between the two antennas is neglected for simplicity of analyse. Performance parameters of the GPR equipment are given in Table 2.

4.2. Data Acquisition Process. The nondestructive GPR field testing of the pile foundation follows seven steps, as shown in Figure 7. Step 1 is running the data acquisition software. After the radar system is connected by cables, by opening the data acquisition K2 FastWave software in the notebook computer, the radar system is activated. The data acquisition software is ready for use after the four indicators in the

(a) (b)

Figure 6: The TR80 antenna. (a) The two antenna and (b) the bonded TR80 antenna.

Table 2: Performance parameters of the GPR device [21].

Pulse repetition frequency	Range	Scan rate	Number of samples per scan	Sample size
400 kHz per channel	Up to 9999 ns	Up to 850 scan/s	128–8192	16 bit
Stacking number	Resolution	Dynamic range	Power consumption	Signal to noise ratio
Up to 32768 scans, automatic or user selection	Better than 5 ps	>160 dB	13 W	>160 dB

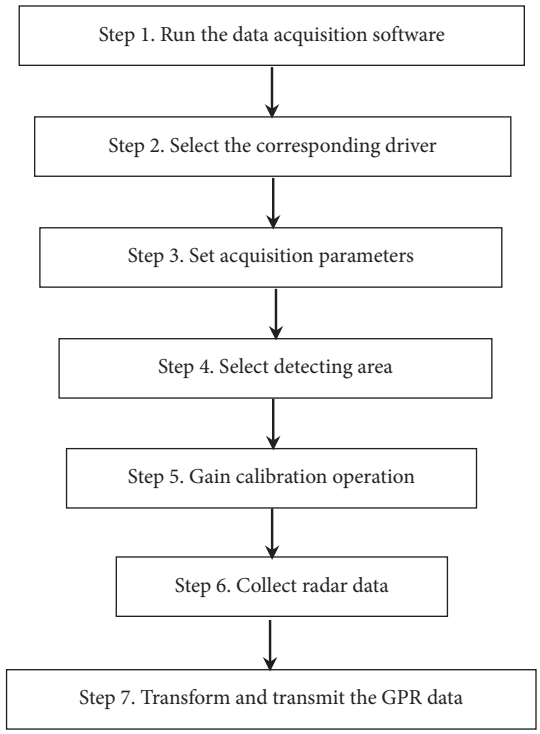

Figure 7: Operation procedure of the GPR field testing.

screen are displayed in green light. Also, the impulse of the antenna is shown in the right corner of the screen, which means the antenna is ready to work. Step 2 is the selection of the driver of the antenna. Since different antennas have different drivers, the driver of the antenna needs to be specified in the software before the GPR survey. Step 3 is the setting of the acquisition parameters. The acquisition parameters need to be set right in the software before the GPR field testing process. The parameters setting of the GPR system is given in Table 3. Step 4 is the selection of the detecting area. The two-dimensional GPR scan is performed along the detection route above the problematic pile foundation. Step 5 is the gaining calibration operation. In order to improve the data quality of the reflected wave signals, automatic gaining calibration is conducted before the GPR field testing to obtain the performance of the inspecting medium. Step 6 is the collection of the reflected GPR wave signals. The electromagnetic wave signals are launched continuously along the detection route, and the feedback wave signals are recorded by the receiving antenna. The last step of the GPR survey is transforming and transmitting the GPR raw data. The recorded wave signals are transformed into digital data in the DAD control element and transmitted to the notebook computer for further processing and analysing. The detected pile foundation was adjacent to a road. The surface of the pile foundation was flush with the road surface. Hence, the GPR antenna was able to move on the road to cover the pile foundation. The radar detecting route was marked as an arrow line above the surface of the pile foundation, as shown in Figure 1(b).

5. Postprocessing of the GPR Raw Data

In order to enhance the essential information, reduce the clutter for clear display, and easy interpretation of the GPR raw data, the GPR raw data were processed with optimized procedures of digital filtering techniques. The radar image of the GPR raw data is shown in Figure 8. The horizontal axis is the distance of movement of the antennas, and the vertical axis is the wave propagation time. As shown in Figure 8, the radar image of the GPR raw data cannot clearly show the

Table 3: Parameters settings of the GPR device.

Centre frequency (MHz)	Total time windows (ns)	AD conversion resolution (bit)	Samples/traces	Trace interval (m)	Marker interval (m)
80	256	16	512	0.02	10

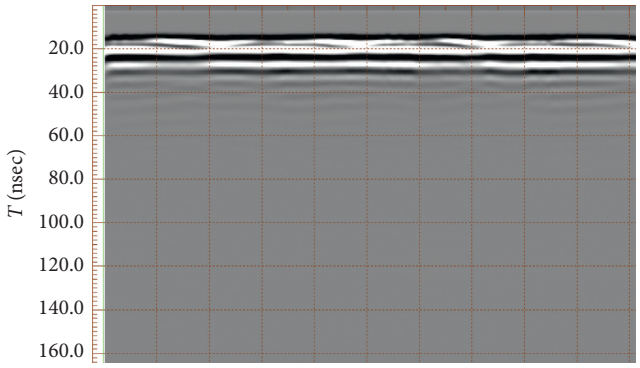

Figure 8: Radar image of the GPR raw data.

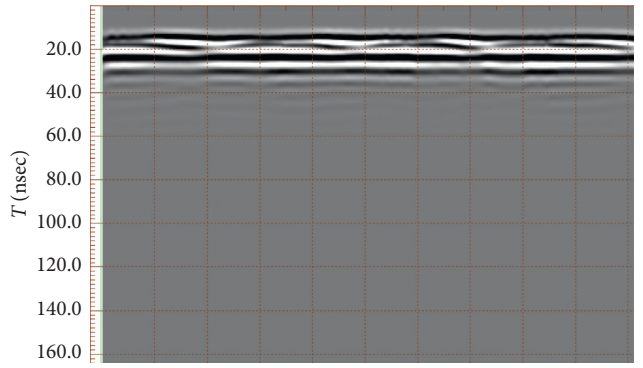

Figure 9: Radar image after the vertical band-pass filtering in time domain.

anomalies in the pile foundation. Digital filtering techniques were employed to process the GPR raw data for observation and interpretation of the radar image. The proposed post processing method of the GPR field testing raw data has four steps.

5.1. Vertical Band-Pass Filtering in the Time Domain. Vertical band-pass filter in the time domain was applied first to the GPR raw data to remove the signals in high and low frequencies. Finite impulse response (FIR) filter in the vertical direction was used in this step. A band-pass filter with a low cut frequency of 100 MHz and a high cut frequency of 1000 MHz was applied to remove possible low and high frequency segments from each trace. The radar image after the band-pass filter processing is shown in Figure 9.

5.2. Correction of the Starting Time of the Received Wave Signals. For the purpose of obtaining the depth information of anomalies in the inspecting medium, the starting time of the received wave signals needs to be corrected. The air-medium interface reflection peaks were aligned and set as the starting time of the received wave signals. Each trace was corrected by changing the starting time to the first reflection peak of the received wave signals. By this operation, the wave propagation time in the air was removed in each trace. The depth scale of the radar image was aligned with the position of the surface of the inspecting medium. The radar image after correcting the starting time is shown in Figure 10. As presented in Figure 10, the upper part of the received wave signals were removed, ensuring that the wave propagation time travelling in the air was eliminated.

5.3. Removing the Background Noise. After correcting the starting time of the received wave signals, background noise was removed from the radar data in this step. The background noise removal operation used a default clearing filter

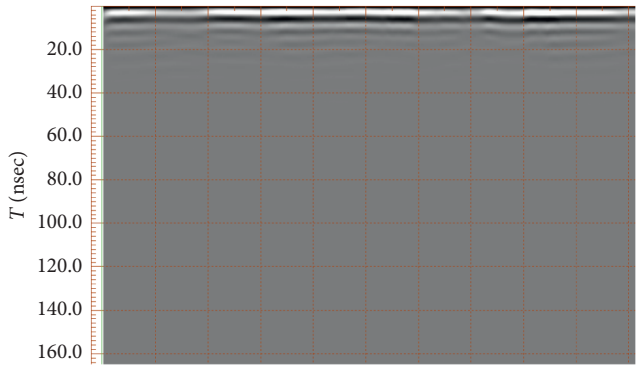

Figure 10: Radar image after the correction of the starting time.

to remove continuous interference components along the horizontal direction, which was caused by horizontal background noise and the ringing effects. The low and high limits of the background noise removal operation were set to a minimum value of 0 and a maximum value of 10 meters. The depth range for background noise removal was set from the surface to the depth of 10 meters. Figure 11 shows the radar image after removing the background noise.

5.4. Linear Gain Operation. The linear gain operation was applied to the received wave signals after removing the background noise. The aim of linear gain operation was to eliminate the attenuation of the received wave signals propagating into the inspecting medium. The linear gain filtering was applied to the wave signals. Equalization of the power energy along the sweep was conducted based on an estimation of the linear trend in the attenuation. The processed data after linear gain operation are shown in Figure 12. The radar image after linear gain operation became clear and explicit to observe and interpret. The longitudinal axis of the radar image is displayed as wave propagation

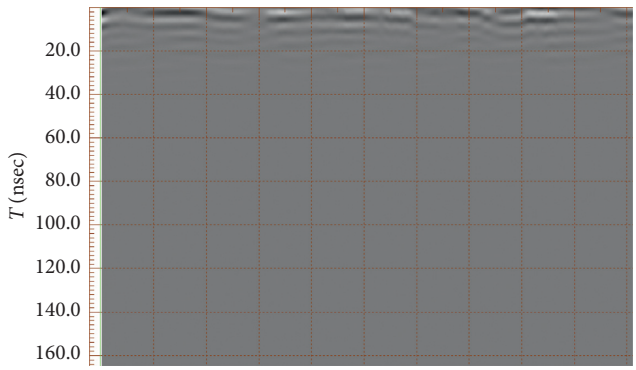

Figure 11: Radar image after removing the background noise.

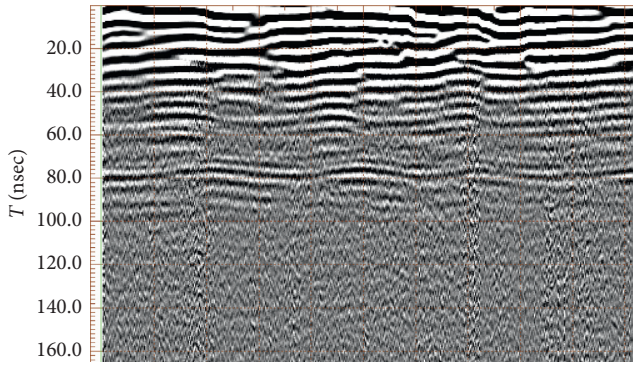

Figure 12: Radar image after the linear gain operation.

time. However, the time must be transformed into depth using the wave velocity to obtain the depth information of the embedded reinforcing bars.

6. Results and Validation

6.1. Estimation of the Electromagnetic Wave Velocity. Figure 13 shows the radar image after the processing of the GPR raw data by using the above digital filtering techniques. The depth is calculated by equation (10) with a hypothetical wave velocity of 100 mm/ns. The wave velocity of 100 mm/ns may not be the true wave velocity in the inspecting medium. Hence, the depth shown in Figure 13 may not be the true depth of the reinforcing bar. In order to determine the true depth of the reinforcing bar from the radar image, the accurate wave velocity in the inspecting medium should be estimated. The determination of the accurate wave velocity is dependent on the hyperbolic signature. The hyperbola match method was used to determine the accurate wave velocity, as described in Section 3.4.

Assuming that the material is homogeneous, a constant value of wave velocity propagating in the inspecting medium can be obtained. The mathematical model of equation (9) was used to generate different hyperbolas corresponding to different wave velocities.

Equation (2) shows that the wave velocity can be determined by the relative dielectric permittivity (ε_r). A broad range of relative dielectric permittivity with the range of $\varepsilon_{r\min}$ and $\varepsilon_{r\max}$ was selected according to the concrete

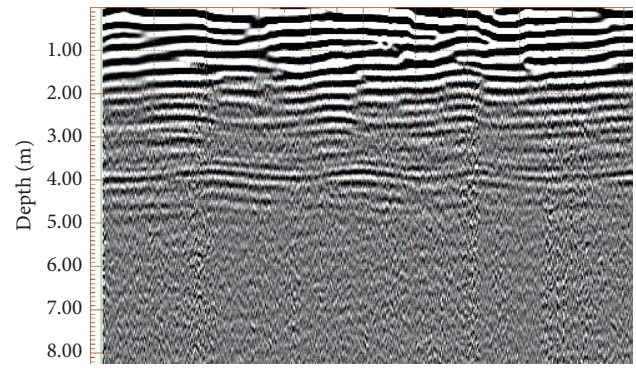

Figure 13: Radar image converted with the default wave velocity of 100 mm/ns.

material, as given in Table 1. After that, the different relative dielectric permittivity was taken into equation (2) to calculate the wave velocities. With the obtained wave velocities, a number of hyperbolic curves were obtained by equation (9). The obtained hyperbolic curves were compared with the coordinates (x_i, t_i), which were extracted from the hyperbolic signature. The direct least square method was used to determine the best match curve based on the lowest fitness function in equation (14).

The accurate wave velocity was determined corresponding to the best match curve. Figure 14 shows the best match curves of two hyperbolic signatures by applying the hyperbola match method, which provided the same results of wave velocity (135 mm/ns). The similar wave velocities from the hyperbola match methods indicate the accuracy of the calculation of wave velocity inversion. The wave velocity of 135 mm/ns was used to calculate the vertical depth using equation (10). The time-depth conversion of the radar image was performed based on the calculated wave velocity.

6.2. Inspection of Reinforcing Bars in the Pile Foundation. Although many GPR profiles were received in the field testing, in this study, the most representative results that illustrated the evaluation are presented. Figure 15 shows the GPR profile, which provides a clear display of the embedded reinforcing bars as hyperbolic signatures. There are two hyperbolic signatures as marked in black rectangle boxes in Figure 15, which are the evidence of the presence of the embedded reinforcing bars in the pile foundation. Also, the depth of the reinforcing bars was estimated after the time-depth conversion of the radar image based on the calculated wave velocity. The GPR testing results indicated that the reinforcing bars were 3.2 meters beneath the surface of the pile foundation.

6.3. Validation of the GPR Testing Results. The pile foundation was excavated based on the GPR testing results. The excavation was performed after the GPR investigation. The pile foundation was excavated to 3.2 meters, and the reinforcing bars were exposed. Figure 16 shows the photos taken from the excavation site. Figure 16(a) shows that a temporary brick lining was constructed for the excavation

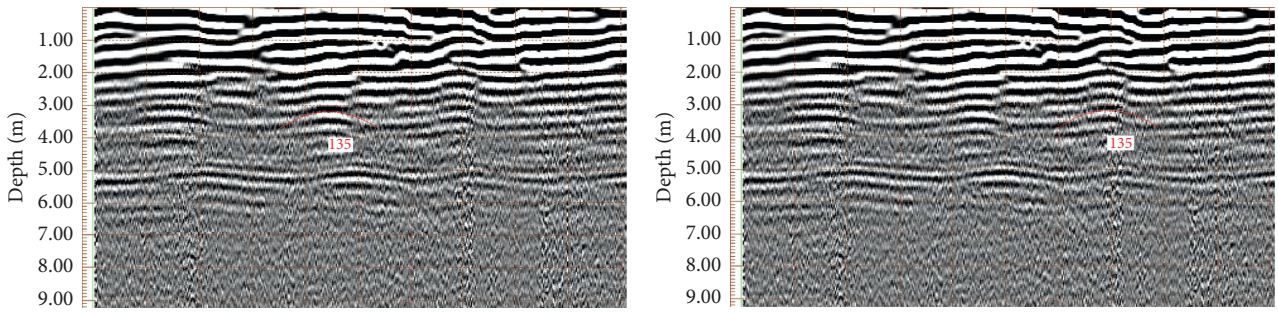

Figure 14: The results of the estimation of wave velocity. (a) First hyperbola match and (b) second hyperbola match.

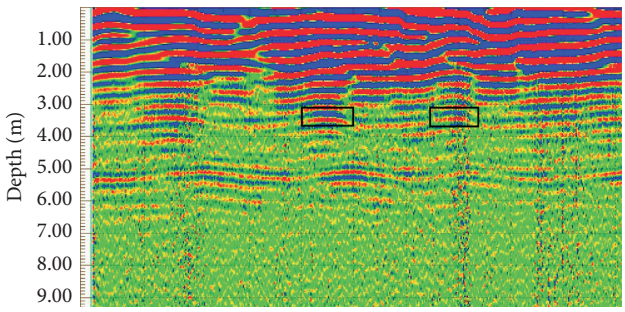

Figure 15: Radar image in a color.

Figure 16: Photos taken from the excavation site. (a) The temporary lining and (b) the exposed reinforcing bars.

surrounding the base of the pile foundation. Figure 16(b) shows the two exposed reinforcing bars.

The actual depths of the embedded reinforcing bars were found to be 3.2 meters, which verified the GPR testing results. The GPR results were found to be accurate in estimation of the deeply embedded reinforcing bars, showing good accuracy. By applying the TR80 antenna with electromagnetic waves in low centre frequency of 80 MHz, the

GPR successfully detected the reinforcing bars located in large depths, and the GPR testing results were validated and confirmed by excavation.

7. Discussion

This study demonstrates the GPR application in the RC pile foundation for the detection of deeply embedded reinforcing bars. The deeply embedded reinforcing bars are in large depths and usually under some other objects. The radar wave signals are attenuated and weakened due to the loss and attenuation for large depth penetration. To solve this problem, low centre frequency antenna of 80 MHz was used to provide high energy waves, which enabled the large depth penetration. It was found that the low centre frequency antenna of 80 MHz could detect the reinforcing bars located at the depth of 3.2 meters in the concrete medium.

The investigated RC pile foundation was adjacent to a road, and the surface of the pile foundation was flush with the road surface. This provided convenience for the GPR field testing. The radar antenna could move on the road along the detection route to cover the surface of the pile foundation. Otherwise, some artificial platforms with continuous pavement for GPR field testing needed to be built, which might increase the cost and enhance the difficulty of the GPR investigation.

The hyperbola match method was used for determining the wave velocity in the pile foundation, and time-depth conversion of the radar image was performed based on the calculated wave velocity. The method is based on the mathematical model of hyperbola, neglecting the bar radius and the distance between the emitting antenna and receiving antenna. It has been found that the hyperbola match method based on these assumptions is effective and provides the wave velocity which leads to the accurate estimation of the depth of the reinforcing bar.

As demonstrated in this study, the GPR can provide information of the location of the embedded reinforcing bar. The information of the embedded reinforcing bar is useful for solving the dispute between the construction unit and the supervision unit. Further treatment of the pile foundation was accepted by the both units. As the depth of embedded reinforcing bar has been determined, the upper segment of the pile foundation with no reinforcement need to be demolished and rebuilt with the designed reinforcement. Different from the traditional method of drilling and excavating, the GPR enables fast survey of the pile foundation in a nondestructive and noninvasive way. The GPR evaluation is important for providing the information of the deeply embedded reinforcing bars, which expand the range of GPR application in civil engineering.

8. Conclusions

A new approach of GPR detection of deeply embedded reinforcing bars is presented in this study. The approach involves GPR field testing, postprocessing of the GPR raw data, and validation of the nondestructive GPR testing results. The GPR field testing was conducted to evaluate the problematic pile foundation. The depth information of the reinforcing bars provided by the GPR evaluation is useful and important in solving the engineering dispute between the construction unit and the supervision unit. The nondestructive hyperbola match method was used to estimate the wave velocity in the inspecting medium. Based on the wave velocity, the depths of the embedded reinforcing bars were estimated. The GPR investigation results were validated with the actual depth of the reinforcing bar in the pile foundation, which was determined through the excavation of the pile foundation.

For large depth penetration, the antenna with low centre frequency waves is essential to provide high energy waves to detect the deeply embedded objects. This study presents the application of TR80 antenna with the waves in the centre frequency of 80 MHz. The TR80 antenna enables to detect the reinforcing bars at 3.2 meters depth located in a reinforced concrete pile foundation.

The radar image after the postprocessing of digital filtering techniques provided a clear display of the embedded reinforcing bars. The digital filtering techniques were fundamental in the postprocessing of the GPR raw data to provide the hyperbolic signature in the radar image. The digital filtering technique made the interpretation of GPR profile feasible.

The hyperbola match method was found to be effective to determine the wave velocity, which led to estimate the accurate depth of the reinforcing bar. The assumptions adopted in the analysis made the calculation process much easier and accurate.

The GPR is proved to be an effective and reliable technique in providing the depth information of the deeply embedded reinforcing bars in the RC pile foundation. The deeply embedded reinforcing bars can be revealed as hyperbolic signature in the processed radar image through the postprocessing procedures. Also, the depth of the deeply embedded reinforcing bars was determined with good accuracy.

Data Availability

The data used to support the findings of this study are available from the corresponding author upon request.

Conflicts of Interest

The authors declare that they have no conflicts of interest.

Acknowledgments

The first author extends his grateful thanks to his colleagues Nianwei Li and Aizhao Zhou who helped to fulfil the testing. Also, the first author would like to thank Jiangsu University of Science and Technology, China, for supporting this study.

References

[1] W. W.-L. Lai, X. Dérobert, and P. Annan, "A review of ground penetrating radar application in civil engineering: a 30-year

journey from locating and testing to imaging and diagnosis," *NDT & E International*, vol. 96, pp. 58–78, 2018.

[2] R. Evans, M. Frost, M. Stonecliffe-Jones, and N. Dixon, "Ground-penetrating radar investigations for urban roads," *Proceedings of the Institution of Civil Engineers-Municipal Engineer*, vol. 159, no. 2, pp. 105–111, 2006.

[3] J. Hugenschmidt, "Concrete bridge inspection with a mobile GPR system," *Construction and Building Materials*, vol. 16, no. 3, pp. 147–154, 2002.

[4] L. Xiang, H.-L. Zhou, Z. Shu, S.-H. Tan, G.-Q. Liang, and J. Zhu, "GPR evaluation of the Damaoshan highway tunnel: a case study," *NDT & E International*, vol. 59, pp. 68–76, 2013.

[5] V. Barrile and R. Pucinotti, "Application of radar technology to reinforced concrete structures: a case study," *NDT & E International*, vol. 38, no. 7, pp. 596–604, 2005.

[6] S. Miramini, M. Sofi, A. Aseem et al., "Health assessment of a pedestrian bridge deck using ground penetrating radar," *Electronic Journal of Structural Engineering*, vol. 1, pp. 30–37, 2018.

[7] M. R. Shaw, S. G. Millard, T. C. K. Molyneaux, M. J. Taylor, and J. H. Bungey, "Location of steel reinforcement in concrete using ground penetrating radar and neural networks," *NDT & E International*, vol. 38, no. 3, pp. 203–212, 2005.

[8] R. Muldoon, A. Chalker, M. C. Forde, M. Ohtsu, and F. Kunisue, "Identifying voids in plastic ducts in post-tensioning prestressed concrete members by resonant frequency of impact-echo, SIBIE and tomography," *Construction and Building Materials*, vol. 21, no. 3, pp. 527–537, 2007.

[9] V. Pérez-Gracia, F. García García, and I. Rodriguez Abad, "GPR evaluation of the damage found in the reinforced concrete base of a block of flats: a case study," *NDT & E International*, vol. 41, no. 5, pp. 341–353, 2008.

[10] P. Wiwatrojanagul, R. Sahamitmongkol, S. Tangtermsirikul, and N. Khamsemanan, "A new method to determine locations of rebars and estimate cover thickness of RC structures using GPR data," *Construction and Building Materials*, vol. 140, pp. 257–273, 2017.

[11] X. Wu, *Technique Manual of Non-Destructive Test of Concrete Structures*, China Communication Press, Beijing, China, 2003, in Chinese.

[12] W. C. Che, H. L. Chen, and S. L. Hung, "Measurement radius of reinforcing steel bar in concrete using digital image GPR," *Construction and Building Materials*, vol. 23, pp. 1057–1063, 2009.

[13] Z. Mechbal and A. Khamlichi, "Determination of concrete rebars characteristics by enhanced post-processing of GPR scan raw data," *NDT & E International*, vol. 89, pp. 30–39, 2017.

[14] W.-L. Lai, T. Kind, M. Stoppel, and H. Wiggenhauser, "Measurement of accelerated steel corrosion in concrete using ground-penetrating radar and a modified half-cell potential method," *Journal of Infrastructure Systems*, vol. 19, no. 2, pp. 205–220, 2013.

[15] M. I. Hasan and N. Yazdani, "An experimental study for quantitative estimation of rebar corrosion in concrete using ground penetrating radar," *Journal of Engineering*, vol. 20168 pages, 2016.

[16] J. H. Bungey, "Sub-surface radar testing of concrete: a review," *Construction and Building Materials*, vol. 18, no. 1, pp. 1–8, 2004.

[17] H. D. Wang, J. P. Deng, J. Luo, and M. Zhang, "Nondestructive monitoring experiments on length of CFG piles by GPR," *Applied Mechanics and Materials*, vol. 90–93, pp. 298–301, 2011.

[18] A. V. Hebsur, N. Muniappan, E. P. Rao, and G. Venkatachalam, "Application of ground penetrating radar for locating buried impediments to geotechnical exploration and piling," *International Journal of Geotechnical Engineering*, vol. 7, no. 4, pp. 374–387, 2013.

[19] *User's Manual of RIS K2-Fastwave a Field Acquisition Unit: Operative Instructions to the Use of RIS K2-Fastwave a Field Georadar System (Version: 3.1)*, IDS Company (Ingegneria Dei Sistemi S.p.A), Pisa, Italy, 2008.

[20] *User's Manual of the Greswin 2 Software Module (Version: 1.0)*, IDS Company (Ingegneria Dei Sistemi S.p.A), Pisa, Italy, 2003.

[21] S. Ebihara, K. Kobayashi, K. Okuhira, and H. Maeda, "3-D estimation of a foundation pile using polarization-sensitive directional borehole radar," in *Proceedings of the IEEE 2017 9th International Workshop on Advanced Ground Penetrating Radar (IWAGPR)*, pp. 1–6, Edinburgh, Scotland, June 2017.